

A hybrid approach to basis set independent Poisson solver for an arbitrary charge distribution

Po-Hao Chang,^{1,*} Zachary Buschmann,¹ and Rajendra R. Zope^{1,†}

¹*Physics Department, University of Texas at El Paso, El Paso, Texas 79968, USA*

We review two common numerical schemes for Coulomb potential evaluation that differ only in their radial part of the solutions in the spherical harmonic expansion (SHE). One is based on finite-difference method (FDM) while the other is based on the Green's function (GF) solution to the radial part of the Poisson equation. We analyze the methods and observe that the FDM-based approach appears to be more efficient in terms of the convergence with the number of radial points, particularly for monopole ($l = 0$). However, as a known issue, it suffers from error accumulation as the system size increases. We identify the source of error that comes mainly from $l = 1$ (and sometimes $l = 2$) contribution of SHE induced by the charge partitioning. We then propose a hybrid scheme by combining the two methods, where the radial solution for $l = 0$ is obtained using the FDM method and treating the remaining terms using GF approach. The proposed hybrid method is subsequently applied to a variety of systems to examine its performance. The results show improved accuracy than earlier numerical schemes in all cases. We also show that, even with a generic set of radial grid parameters, accurate energy differences can be obtained using a numerical Coulomb solver in standard density functional studies.

I. INTRODUCTION

The rapid advancement of computing power has allowed accurate numerical simulations of material properties for more realistic and complex systems under first-principles-based approaches. Although DFT is the most widely applied quantum mechanical method, as it offers the best balance between the accuracy and the computational cost, the evaluation of Hartree contribution to the Hamiltonian that describes the classical part of electron-electron interactions remains one of the major numerical challenges. Therefore, it is crucial to be able to determine Hartree energy efficiently and accurately.

In of computational quantum chemistry, Gaussian type orbitals (GTOs) are among the most popular basis sets as they benefit from the analyticity of Gaussian product rules and of their integrals which allows various integrals like the basis overlap integrals, Coulomb integral, exchange integrals, dipole integrals etc. to be evaluated efficiently and analytically [1].

Over the years, many efficient schemes have been developed around GTOs to tackle computationally costly two-electron integral in Coulomb problems. [2–17] Starting from the Boys function for Coulomb potential due to a spherically symmetric Gaussian charge distribution, the potential due to charge involving higher angular momentum components can be efficiently constructed recursively. The most common recursive schemes are the ones proposed by McMurchie and Davidson [2] and Obara and Saika [3]. These common GTO integral evaluations have been implemented in integrals libraries such as libint and libcint [18, 19] which are at the heart of many software packages.

Despite the fact that the recursive schemes improve the performance significantly, the poor scaling of 4-center integrals is still inherently problematic. In order to achieve

a better scaling, follow up on the idea of combining numerical grid and a finite basis set [4], Termath and Handy proposed to analytically evaluate the Coulomb potential on a numerical grid [9]. Not only does this approach drastically reduce the complexity, the idea can also be further combined with either standard far-field expansion [20] or efficient and accurate algorithm such as faster multipole method FMM and tree codes [10–15]. The advantage becomes particularly obvious when it involves higher angular momentum basis functions.

A pure numerical basis-set-free approach to the Coulomb problem in polyatomic systems was first proposed by Becke and Dickson [21]. The method utilizes multi-center numerical grid [16], proposed also by Becke the same year, that partitions the space into multiple regions. Such partitioning of space allows the integration within each region to be performed independently by solving the Poisson equations for the charge density confined in each region. By combining with multipolar expansions, one can then obtain a set of radial part of the Poisson equations. Once the radial equations are solved, the solutions can be used to construct Coulomb potential in the form of spherical harmonic expansion (SHE).

The approach is appealing but unfortunately suffers from accuracy issues when it comes to more spatially extended large molecules as the error per atom appears to be accumulative [9]. This limits the the method from being applied to larger size systems. The extensive literature search revealed that only a handful of implementations [9, 22–24] adopted this method and majority of these works only focused on small molecules [23–27].

Shortly after, based on the same theoretical framework, Delley used the integral form of the Green's function (GF) solution to the Laplacian [17] as an alternative to solve the radial part of the Poisson equations. This approach removes the problem of error accumulation with

system size, thereby opening a gateway to broader numerical Poisson applications. The method is now more widely used and has been implemented in a few DFT codes [28, 29] for large scale calculations.

The numerical Poisson solver based on multi-center grid and multipolar expansion has been discussed in several earlier works and shown promises. But it is mostly adopted in grid [24], Slater-type orbital (STO) [30, 31] or numerical atomic orbital (NAO) based codes [29, 32], and rarely applied to Gaussian-based DFT codes as the Coulomb potential can already be calculated analytically [2, 3]. There have been only a handful of earlier works that attempted at applying the numerical Poisson solver to GTO based first-principles calculations on rather small systems (i.e. mostly less than 10 atoms).

However, numerical Coulomb has several advantages, besides being basis set independent. In a Gaussian based approach, it can be particularly efficient when dealing with heavier elements with a large basis set that involves higher angular polarization functions. It can also be combined with far-field multipole expansion naturally for a more efficient computational scaling. Since each center is treated independently, it also be parallelized easily for large scale calculations [28, 31].

Our interest in the basis-set-free numerical scheme stems from the limitation in using the standard analytic scheme for calculation of Coulomb potential of the scaled charge density needed in fully self-consistent implementation of the locally scaled self-interaction-correction (LSIC) method developed by some of us. The LSIC method identifies the one-electron self-interaction regions with the help of an iso-orbital indicator and determines the magnitude of SIC at each point according to the value of iso-orbital indicator [33]. The LSIC method which was earlier applied in a perturbative manner using the self-consistent Perdew-Zunger SIC (PZSIC) orbitals, have shown remarkable improvement over the well known PZSIC method for many properties [33]. It is the first one-electron SIC method that provides the atomization of energies of AE6 database that are more accurate than the Perdew-Burke-Erzerhof generalized gradient approximation without spoiling the accuracy of barrier heights. This work also showed that major errors made by the LSDA functional can be removed by removing self-interaction errors using LSIC like approach. The self-consistent implementation of LSIC method is therefore important and the present work, which will allow calculation of Coulomb potential of a charge density scaled by an iso-orbital indicator is, the first step towards the self-consistent LSIC.

The manuscript is organized as follows: we first review two major methods [17, 21]. Then we performed a series of tests along with some numerical tricks to enhance the radial grid efficiency. By analyzing and comparing the data for both methods we were able to identify the origin of the strengths and weakness in both methods. Finally,

we propose a hybrid approach to further optimize the performance of the numerical Poisson solver.

II. METHOD REVIEW

A. Mesh generation

The numerical Poisson solver utilizes so called multi-center grid [16], or often collectively referred to as Becke mesh, that was originally designed for 3D molecular integrals for functionals of the form $F(\rho(r), \nabla\rho(r), \nabla^2\rho(r))$. To properly described the cusps at the nuclear cores, the grid itself is constructed as a superposition of multiple spherical integration grids where each spherical grid is constructed by multiplying a radial quadrature onto a spherical mesh to form concentric spherical shells of mesh centered on each atomic site.

While Lebedev quadrature is generally believed to be the most efficient for spherical mesh [34], there have been a wide variety of options for choosing radial grids [35–43], and each has its own advantages. In this study we adopt the radial quadrature proposed by Mura and Knowles [41], as it has been proven to be numerically efficient [38] and has a simple form

$$r_i = -\alpha \ln(1 - x_i^m) \quad (1)$$

where

$$x_i = \frac{i}{N+1}, \quad i = 1, 2, \dots, N \quad (2)$$

N is the number of radial points, and both α and m are empirical parameters controlling how the points are distributed. The recommended values are $m = 3$ and $\alpha = 5.0$ (7.0 for alkali and rare-earth metals) [40].

This simple expression makes it easier for analytically evaluating the coefficients of the FDM operator for solving 1D radial Poisson equations.

B. Partition functions

The overlap between the meshes from different centers can be avoided by scaling down the integrated function $\rho(r)$ with the partition weight function w_n as

$$\rho_n(r) = \rho(r)w_n(r) \quad (3)$$

and

$$\rho(r) = \sum_n \rho_n(r)w_n(r). \quad (4)$$

Below we refer to this process as single-centerization where the whole space is partitioned into multiple independent cells, similar to the Voronoi cells but with smoother transition boundaries and each cell contains only one nucleus.

The relative weight functions w_n are constrained to satisfy the condition

$$\sum_n w_n = 1 \quad (5)$$

and defined as

$$w_n(r) = \frac{\mathcal{P}_n(r)}{\sum_{m=1}^{N_{\text{atoms}}} \mathcal{P}_m(r)} \quad (6)$$

where $\mathcal{P}_n(r)$ is the cell function.

Over the years, many cell function generating schemes have been proposed. Begins with the original one proposed by Becke [16] that requires predetermined empirical parameters to accommodate different atomic species of different sizes. Delley [17] provides some easier atomic density dependent implementations to naturally account for the molecules that contain different atomic species. Some weight schemes are also proposed to achieved better scaling for finite systems [44] and for periodic systems [31]. There are also variants based on Becke's original scheme which are designed for certain properties of interests [45, 46].

Although the mesh generated with these cell function schemes can be applied to both general 3D molecular integration and numerical Poisson solver, they are not necessary the same [17]. The weight functions constructed with different cell functions are generally in good agreement, however our experience suggests that the scheme proposed by Stratmann [44] gives the most accurate results in some geometries which confirms the earlier report [29]. Therefore the Stratmann's approach is adopted for all the calculations presented in this current study.

C. Single centerization and multipolar expansion

The starting point is to replace the source term in Poisson equation with a single-centered charge defined in Eq. 3. This results in significant simplification as one only needs to deal with the equation containing one atomic center at a time.

$$\nabla V_n(r) = -4\pi\rho_n(r). \quad (7)$$

As the mesh for each center is constructed based on spherical mesh, we can efficiently expand both ρ_n and V_n with spherical harmonic functions [20] respectively as

$$\rho_n(r, \theta, \phi) = \sum_{lm} \rho_{lm}^{(n)}(r) Y_{lm}(\theta, \phi) \quad (8)$$

and

$$V^{(n)}(r = |r' - r_n|, \theta, \phi) = \sum_{lm}^{l_{max}} V_{lm}(r) Y_{lm}(\theta, \phi), \quad (9)$$

where

$$\rho_{lm}^{(n)}(r) = \int_{\Omega} \rho_n(r, \theta, \phi) Y_{lm}(\theta, \phi) d\Omega \quad (10)$$

and $V_{lm}^{(n)}(r)$ are to be solved.

D. Radial Poisson

For each lm component in SHE, the angular and radial degrees of freedom are separable, the Poisson equation can then be converted into a set of 1D problems. There are two major approaches to solve for V_{lm} which is where Delley and Becke's methods differ.

In Becke's approach, $V_{lm}(r)$ are obtained by solving a set of 1D differential equations. With the substitution

$$V_{lm}(r) = \frac{U_{lm}(r)}{r},$$

one arrives at the following general expression

$$\frac{\partial^2}{\partial x^2} U_{lm}(r) + p(r) \frac{\partial^2}{\partial x^2} U_{lm}(r) - q(r) U_{lm}(r) = f(r), \quad (11)$$

where

$$x_i = (1 - \exp(-r_i/\alpha))^{\frac{1}{m}}. \quad (12)$$

Eq. 11 can be solved using FDM with the coefficients calculated through

$$p(r) = \frac{\partial^2 x}{\partial r^2} / \left(\frac{\partial x}{\partial r} \right)^2, \quad (13)$$

$$q(r) = \frac{l(l+1)}{r^2 \left(\frac{\partial x}{\partial r} \right)^2} \quad (14)$$

and

$$f(r) = -4\pi\rho_{lm}(r) / \left(\frac{\partial x}{\partial r} \right)^2. \quad (15)$$

The boundary conditions (BCs) are imposed to be $U_{lm}(r) = 0$ for $r=0$ and $r \rightarrow \infty$ for all lm 's except for the monopole $l = 0$ where $U_{00}(r \rightarrow \infty) = \sqrt{4\pi}q_n$.

On the other hand, Delley applied the GF solution to the Laplacian [47] to integrate with charge directly for $I_{lm}(r_i)$ [17, 28, 29] in the following form

$$I_{lm}(r_i) = \frac{1}{r_i^{l+1}} \int_0^{r_i} r'^{l+2} s_{lm}^i(r') dr' + r_i^l \int_{r_i}^{\infty} \frac{s_{lm}^i(r')}{r'^{l-1}} dr'. \quad (16)$$

where s_{lm}^i is the fitted charge density evaluated at mesh point r_i .

In this study, we also try to further smooth out the fitted curve $s_{lm}^i(r')$ by rearranging the integral form of both terms in Eq. 16 into the following expression

$$I_{lm}(r_i) = \frac{1}{r_i^{l+1}} \int_0^{r_i} r'^{l+2-p} [r^p s_{lm}^i(r')] dr' + r_i^l \int_{r_i}^{\infty} \frac{[r^p s_{lm}^i(r')]}{r'^{l-1+p}} dr' \quad (17)$$

where $p = 0, 1$ or 2 and we perform cubic spline interpolation on $[r^p s_{lm}^i(r')]$ instead. The solution of the radial Poisson defined in Eq. 9 can be expressed as

$$V_{lm}(r) = \frac{4\pi}{2l+1} I_{lm}(r).$$

This approach is in principle straightforward, however the integration for Eq. 16 and 17 is tricky, as the integration is done for every r_i and can no longer benefit from the quadrature weights. The numerical instability could potentially occur in both the interpolation of the charge and the evaluation of Eq. 16 as the term involves higher order polynomial terms. In some of the earlier works such as Ref. [29], the integration is first evaluated by spline-interpolating the multipolar charge density onto a denser mesh and then the integration is done numerically. Here, we adopt the most recent Franchini's integration scheme [28] instead where the multipolar charge density, $s_{lm}^i(r)$ at interval $[i, i+1]$, is expressed as piece-wise polynomials

$$s_{lm}^j(r) = a_j + b_j r + c_j r^2 + d_j r^3 \quad (18)$$

then the integrals in Eq. 16 can be evaluated analytically for each segment. This approach should, in principle, yield the most accurate results for a given spline compared to the former and is also computationally more efficient.

E. Reconstructing the Coulomb potential

Once the 1D radial solutions V_{lm} are calculated, the total Coulomb potential due to the charge in a particular cell can be reconstructed on any integration mesh using Eq. 9, where $V_{lm} = r^{-1} U_{lm}(r_i)$ for Becke's FDM and $V_{lm} = \frac{4\pi}{2l+1} I_{lm}(r_i)$ for Delley's GF integral. For V_{lm} of any arbitrary given r' that does not coincide any radial grid point r_i , the evaluation is done using cubic spline interpolation

$$V^{(n)}(r_i = |r' - r_n|, \theta_i, \phi_i) = \sum_{lm}^{l_{max}} V_{lm}^{interp}(r_i, \theta_i, \phi_i). \quad (19)$$

F. Screening charge

As the charge density $\rho(r)$ normally possesses rapid changing peaks in the proximity of nuclei, it is often useful to introduce some type of screening charge [17, 29]. The ρ_{screen} is usually chosen to smooth out the curve around the cusps in $\rho(r)$ and that its corresponding Coulomb potential can be evaluated analytically and efficiently. In which case we only need to consider the Poisson problem due to the variation from the screening charge. A convenient option is the superposition of spherically symmetric neutral atomic charge densities [17, 29].

$$\Delta\rho(r) = \rho(r) - \sum_{\text{sites}} \rho_{\text{atoms}}(r), \quad (20)$$

and the final total Coulomb potential can be restored by adding the analytically evaluated potential V_{atoms} due to the screening charge,

$$V = \Delta V + V_{\text{atoms}}. \quad (21)$$

III. COMPUTATIONAL DETAILS

We use Pederson-Porezag basis set [48] in all our calculations. For the integration mesh, and for the numerical Poisson solver, Lebedev unit sphere quadrature of order $l = 47$, which contains 590 points, is used. For FDM, instead of 7-point suggested by Becke and Dickson [21], we use 11-point central difference formula for the middle radial points and non-central difference for the points involve the boundary to preserve the banded shape of the operator matrix. However we observed that there is no noticeable difference beyond 7-point. The coefficients for FDM operators are generated using Matlab function [49]. For the GF approach of solving radial Coulomb potentials, we adopted Franchini's density fitting [28] with a slight modification as introduced in Eq. 17. For the interpolation of V_{lm} onto any given radial point r , we apply piece-wise cubic spline interpolation subroutine modified from the subroutines in numerical recipes [50].

As the treatment for the angular part of the solutions is well-defined within SHE, the main purpose of this study will be focusing on improving the radial solutions, we choose a generic set of parameters $\alpha = 6$ and $m = 3$, similar to the recommended values in Ref. [41], for the radial quadrature in all our calculations unless explicitly stated.

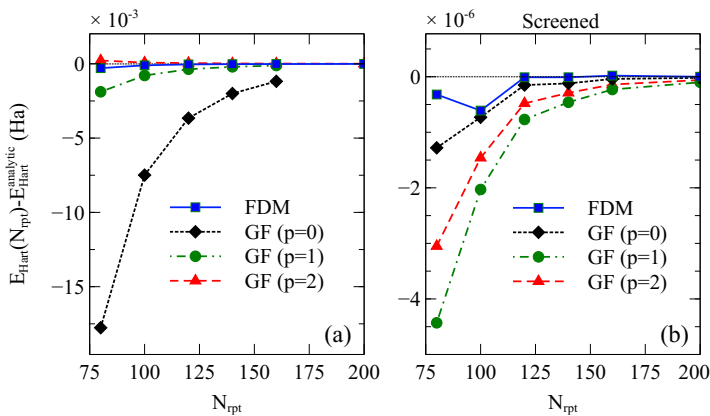


FIG. 1: Hartree energy E_{Hart} for a single Mn atom is calculated using both FDM and GF (a) without and (b) with screening charge. Different modifications of charge interpolation are also performed as a comparison as shown for $p = 0, 1$ and 2.

IV. ANALYSIS AND DISCUSSION

A. Atomic system (single-center)

We begin with the analysis using both methods on single atom systems. As the space partitioning is not required, we get a better grasp of how efficiently the methods perform with respect to a given radial quadrature. Fig. 1 shows the error of Hartree energy for Mn atom (a) without and (b) with charge screening compared to the reference value, where the Coulomb potential is analytically evaluated [9].

From Fig. 1(a), in their primitive form, FDM shows a clear advantage over GF ($p = 0$), as it requires less than 120 radial points to reach 10^{-5} Hartree accuracy while GF provides barely a mHartree accuracy. However, once we have introduced the additional polynomial r^p ($p = 1$ and 2) as defined in Eq. 16 to smooth out the density peak close to the origin, the performance of the GF improves drastically. Particularly with $p = 2$, the GF result is almost comparable with FDM. This suggests that the charge density variation appears to be too large for the cubic spline polynomials to describe the nucleus region as efficiently, and smoothing out the curve reduces the interpolation error.

Fig. 1(b) shows the results when screening charge is applied. Without surprise, with the inclusion of screening charge that naturally reduces the curvature of charge density near the nucleus, the error for both methods are greatly reduced to about 10^{-7} Hartree, with only about 100 points. It is obvious that FDM still outperforms all the GF cases with different p 's, even though the accuracy gap has become much smaller. It is also interesting to note that in this particular case, $p = 1$ or 2 does not

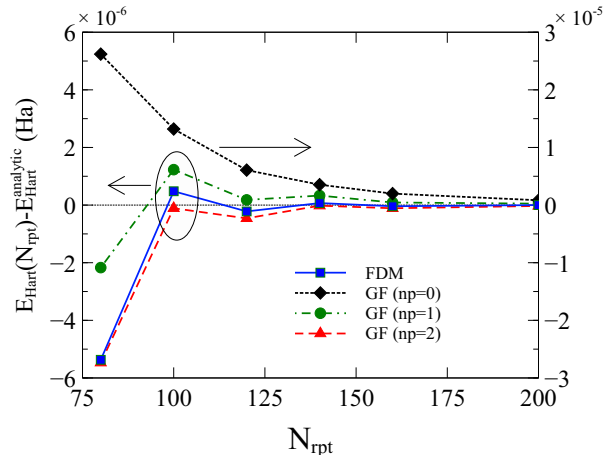


FIG. 2: The error of Hartree energy for a single Cu atom versus number of radial points N_{rpt} of modified charge interpolations (i.e. $r^p s_{lm}^i$ with different shown. Generally, the best performance can be achieved with $n = 2$.

seem to improve the result at all.

Fig. 2 presents the same analysis as Fig. 1 (b) but on a single Copper atom. Please note that the black dashed line for GF ($p = 0$) follows the axis to the right of a larger energy scale, while the other three follow the left axis. By applying screening charge, all four cases offer adequate accuracy with 100 radial points (i.e. $\leq 10^{-5}$ Hartree). Noticeably, the error of FDM is still smaller than all three GF cases, while the result of GF improves as p increases, especially when compared to its original form ($p = 0$) where the error is at least an order of magnitude larger than the rest.

In this case, opposite to the Mn atom, the polynomial factor improves the accuracy even in the presence of screening charge. Although both screening charge and r^p can improve the interpolation, it is still possible that the piece-wise cubic spline is not sufficient, as it incorporates only two adjacent data points (i.e. radial quadrature) for each segment, while FDM naturally incorporates multiple data points during the $2N+1$ -point ($N = 5$) difference operator construction. As a result, FDM is always more accurate with a more stable convergence even without screening charge.

In principle, the result for GF can be further improved by optimizing radial parameters α and m . However, the purpose of this analysis is to demonstrate the effectiveness of the FDM, where the method generally describe the monopole better, and is less sensitive to the radial quadrature parameters. This is particularly useful for solving for the potentials due to orbital densities needed in the self-consistent one electron self-interaction methods [33, 51–53] where suitable screening charges are either

Molecule	E_{Hart}	ΔE		
	Analytic	FDM	GF	Hybrid
Glycine(10)	549.790197	-2.18E-04	8.30E-06	-4.98E-06
Benzene(12)	311.939018	-2.71E-04	1.40E-05	5.01E-06
Decanol(33)	816.263155	-3.54E-04	1.00E-05	3.47E-06
Pentacene(36)	1892.400793	-8.97E-04	2.53E-05	8.54E-06
C ₆₀ (60)	9436.4919523	-1.69E-03	5.45E-05	1.28E-05

TABLE I: Error/atom for a set of testing molecules of different sizes range from 10 to 60 atoms

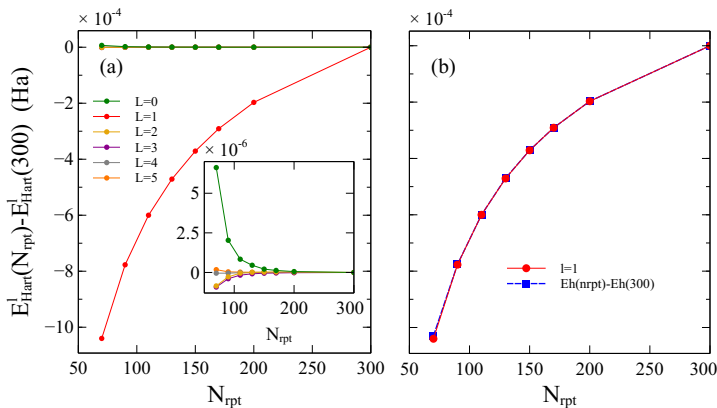


FIG. 3: The deviation of Hartree energy of Glycine molecule of each l -component from the the same quantity but evaluated with $N_{rpt} = 300$ as a convergence test. (a) The Hartree energy contributions from the lowest six orders ($l = 0 \sim 5$). (b) the largest error contribution ($l = 1$) compared to the error of the total Hartree energy.

difficult or expensive to find.

B. Molecular system (multi-center)

Although FDM appears to be very efficient for the single atom case that contains only one center, the situation reversed in the multi-center systems (i.e. molecules). Table I shows error per atom for different radial Poisson solvers on several selected molecules ranging from 10 to 33 atoms. One can see that the FDM becomes particularly problematic. Not only is the error generally large, it also scales with the system size. As previous studies have already pointed out [9], the error appears to be accumulative and becomes worse with increasing system size. The increasing error with system size has limited the method from being used widely.

Furthermore, we also noticed that the result is very sensitive to the radial mesh scaling factor α . An unreasonably large α often yields better accuracy than a small

N_{rpt}	$l = 0$	$l = 1$	$l = 2$	$l = 3$	$l = 4$	$l = 5$
70	1.84E-05	-1.38E-03	-3.96E-07	-2.98E-06	-1.42E-06	-4.18E-07
90	6.75E-06	-1.03E-03	-9.24E-08	-1.10E-06	-5.13E-07	-1.64E-07
110	2.38E-06	-8.00E-04	-5.00E-08	-4.97E-07	-2.34E-07	-7.71E-08
130	1.21E-06	-6.27E-04	-1.97E-08	-2.47E-07	-1.18E-07	-3.81E-08
150	6.80E-07	-4.94E-04	-1.60E-08	-1.31E-07	-6.07E-08	-1.86E-08
170	4.19E-07	-3.88E-04	-3.55E-09	-8.36E-08	-3.77E-08	-1.18E-08
200	2.09E-07	-2.62E-04	-1.45E-09	-3.99E-08	-1.78E-08	-5.90E-09

(a) FDM

N_{rpt}	$l = 0$	$l = 1$	$l = 2$	$l = 3$	$l = 4$	$l = 5$
70	-1.24E-03	-1.04E-04	-1.20E-05	-3.64E-06	-2.10E-06	1.03E-06
90	-4.63E-04	-3.84E-05	-4.38E-06	-1.42E-06	-8.32E-07	3.11E-07
110	-2.09E-04	-1.72E-05	-1.98E-06	-6.64E-07	-3.93E-07	1.18E-07
130	-1.06E-04	-8.72E-06	-9.94E-07	-3.35E-07	-2.05E-07	5.31E-08
150	-5.84E-05	-4.81E-06	-5.47E-07	-1.77E-07	-1.10E-07	2.95E-08
170	-3.40E-05	-2.79E-06	-3.20E-07	-1.13E-07	-6.60E-08	1.72E-08
200	-1.59E-05	-1.31E-06	-1.50E-07	-5.21E-08	-3.20E-08	7.17E-09

(b) GF ($p = 0$)

TABLE II: The l -resolved energy convergence for the Glycine molecule of (a) FDM and (b) GF method versus number of radial points.

one with larger N_{rpt} . This is rather counter-intuitive. Since FDM performs so well in the single atom systems which means the solver is capable of describing the monopole that contains the sharpest peak. Naively, one would expect the charge partitioning should mostly affect the multipolar expansion (i.e. requires larger l).

Table II shows the convergence of the l -resolved Hartree energy contributions for Glycine which is defined as $\Delta E_{Hart}^l(N_{rpt}) = E_{Hart}^l(N_{rpt}) - E_{Hart}^l(300)$, where

$$E_{Hart}^l = \frac{1}{2} \int \rho(r) V_n^l(r) dr$$

is evaluated from the potential defined as

$$V_n^l(r) = \sum_{m=-l}^l V_{lm}(r) Y_{lm}(\theta, \phi).$$

The data reveal something rather intriguing. Particularly in FDM, a perfect convergence trend can be seen in all terms except for $l = 1$ which exhibits at least 3 ~ 4 orders of magnitude larger error than other l components. The result in Table IIa for FDM is also plotted in Fig. 3 for better visualization. From Fig. 3(a), it becomes obvious that the error is entirely coming from $l = 1$ while

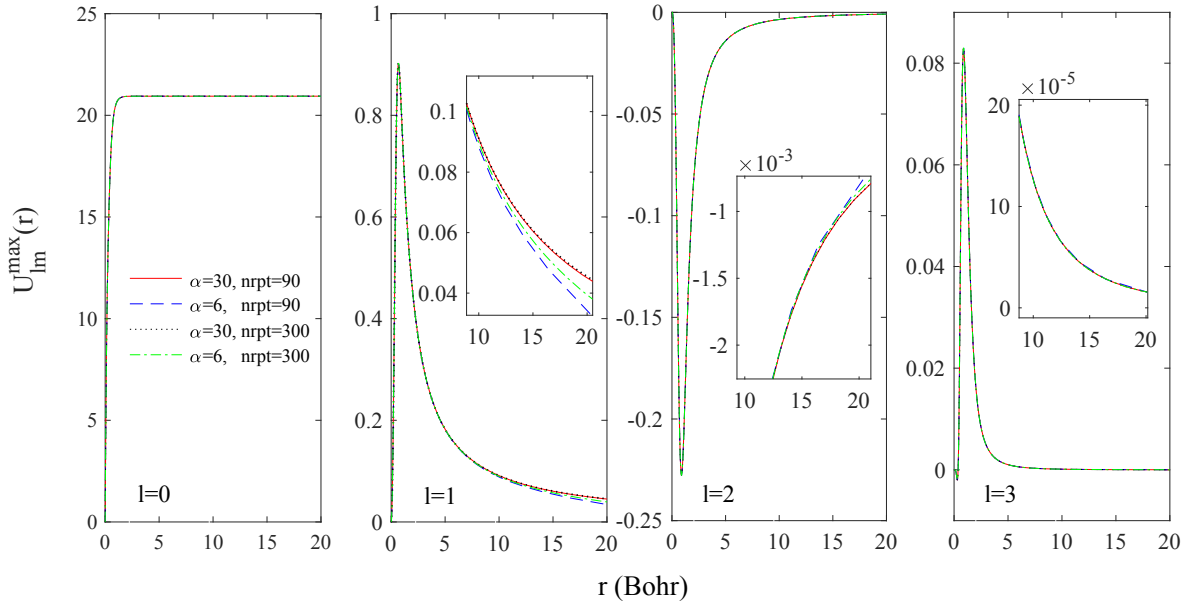


FIG. 4: Four sets of radial parameters are used to test the convergence of the radial solutions. The maximum component of the radial solutions (U_{lm}^{max}) of the four lowest expansion orders (up to $l = 3$) for the oxygen site in Glycine molecule are shown as (a)-(d). For (b)-(d) the insets present a closer look of the convergence of the tails.

all other terms converge rapidly to 0, even the dominant $l = 0$ term is well converged around $N_{rpt}=100$. Fig. 3(b) compares the error only from $l = 1$ and the error of the entire Hartree energy. The two curves coincide nearly perfectly which further confirms not only that $l = 1$ is the only main source of error but also that the contributions from all the higher orders terms converge perfectly.

To better understand this rather peculiar cause of error, we analyze the radial part of the potential, U_{lm} , for the Oxygen site in the Glycine molecule of the lowest four orders as shown in Fig. 4 using four very different sets of radial mesh parameters. Since not all terms are nonzero due to symmetry consideration, only the largest contribution is shown for every l . The parameters (α, N_{rpt}) for each of the four quadratures are chosen as $(6.0, 90)$, $(6.0, 300)$, $(30.0, 90)$ and $(30.0/300)$. A large number radial points $N_{rpt} = 300$, is chosen here intended as an accurate reference. A large scaling factor α simply stretches out the radial mesh to cover wider space range and as a result will make the mesh grid sparse. At the first glance, all four radial meshes coincide nicely at $l = 0$ and $l = 4$ (and the same for all the higher order terms not shown here). On the other hand pronounced deviation in $l = 1$ and a very small but noticeable difference in $l = 2$ can be seen, which indicates that these two l -orders are more sensitive to the radial grid. Upon closer inspection, only the ones with the larger α have converged for $l = 1$ regardless what N_{rpt} is. This means that $N_{rpt} = 90$ is sufficient to describe the region around nucleus and the maximum range of the quadrature $r_{max} = r_{N_{rpt}}$, scaled

directly by α (see Eq. 1) has a significant influence on the accuracy.

Without surprise, $(6, 300)$ gives a better result than $(6, 90)$, but this is partly because the increase of N_{rpt} also increases the r_i^{max} ($=20.5395$ for $(6, 90)$ and $=27.6709$ for $(6, 300)$), rather than the fineness of the mesh. It is now clear that the source of discrepancy is about how the asymptotic behavior is described by FDM rather than the description of the nucleus core region. By looking at the asymptotic tails at a larger distance $r = 20$, U_{lm}^{max} for both $l = 0$ and $l = 4$ (and above) have reached their asymptotic limit $\sqrt{4\pi}q_n$ and 0 respectively. On the other hand for $l = 1$, $U_{1m}^{max}(r = 20)$ is still large and decreasing to 0 in an extremely slow pace (roughly $1/r$), hence induces a large deviation. For the $l = 2$ term, there is a visible but much smaller deviation at $r = 20$, therefore leaves smaller room for discrepancy compare to $l = 1$.

Intuitively speaking, if $U_{lm}(r)$ at the largest radial distance $r = r_{N_{rpt}}$ has not yet approached close enough to the asymptotic value (i.e. $\sqrt{4\pi}q_n$ for $l = 0$ or 0 for $l \neq 0$), a significant error is expected, as FDM only knows the boundary condition at the infinity, the behavior beyond the last radial point $r_{N_{rpt}}$ can only be extrapolated from the last few radial points. This explains why a significant error only emerges in the lower order terms but not $l = 0$, as it reaches $\sqrt{4\pi}q_n$ rapidly within merely few Bohr's, while higher order terms are less likely to suffer from this since they are shorter in range and decay to 0 much faster.

This also explains why the method still works well for

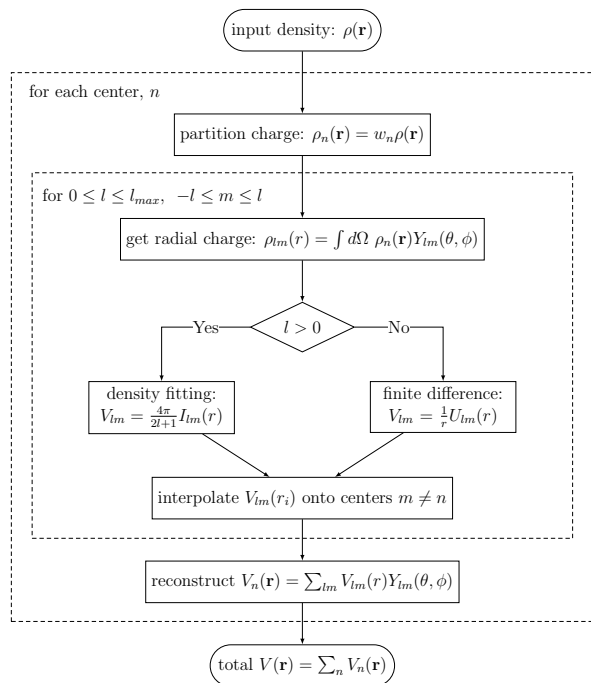


FIG. 5: The flow chart of the numerical Poisson solver.

smaller molecules, as the deviation in the $l = 1$ term in Fig. 4 is not obvious until r is large enough. It is also worth mentioning that in the original attempt, Becke uses Gauss–Chebyshev formula of the second kind for the radial quadrature, which is known to emphasize too much in the extended region while not putting enough points into the chemical bonding region [38]. However, despite not being integrationally optimal, using this quadrature could potentially mitigate the boundary issue appears in U_{lm} terms described above, particularly for smaller size systems.

C. Hybrid radial solver

As discussed in the previous section, the FDM method struggles for $l = 1$ and possibly $l = 2$. On the other hand, GF method only requires the evaluation of charge integrals of the form $r^{k(l)} \rho_{lm}(r)$ (see Eq. 16 and 17), where k is just some integer depends on l chosen manually and does not suffer from the same “boundary” issue. GF generally converges rather nicely with the number of the radial points for all terms except for $l = 0$ as shown in the Table II. This is because the charge density in each center is more localized in space after the truncation imposed by the weight function.

By considering the strengths of both methods, we propose a hybrid approach where FDM is used for the “near-field” $l = 0$ and the rest are calculated using GF integration. The detail of the procedure is outlined in Fig. 5. For a large system, the first term of Eq. 17 which

	p-C ₈ H ₈		Cu ₂ Cl ₆ ²⁻	
	E_{analytic}	ΔE	E_{analytic}	ΔE
E_{BS}	-306.704861	1.19E-04	-6028.542708	-6.80E-06
E_{HS}	-306.698685	1.22E-04	-6028.541461	-7.00E-06
$E_{\text{BS}} - E_{\text{HS}}$	-0.006176	-2.90E-06	-0.001247	2.00E-07
Error (%)		-0.02%		0.01%

TABLE III: Total energy and the total energy difference between high spin and broken symmetry states for p-C₈H₈, and Cu₂Cl₆²⁻. All energies are in unit of Hartree

corresponds to the far-field multipole expansion, is employed to ensure the asymptotic behavior is accurately preserved. In the rest of the discussion, the screening charge is applied to all the calculations unless explicitly stated.

The test used in analysis of FDM and GF method, is also used to analyze the performance of the proposed hybrid approach. The results are shown in Table I. It is evident from the Table that using the same generic set of parameters $(\alpha, N_{rpt}) = (6.0, 90)$, the accuracy of the proposed hybrid approach is improved by several times to an order of magnitude compared to the GF method. More importantly, the error per atom in the proposed hybrid approach does not scale with the system size. According to our analysis, both FDM and GF describe higher order terms (i.e. $l \geq 3$) equally efficient and accurately. Therefore, one would expect to see the same improvement for FDM-based method as long as $l = 1$ terms are calculated using GF.

Energy difference between different spin states

As an assessment of accuracy of the proposed hybrid in practical DFT calculations, we compute the energy difference between different spin states, namely high spin (HS) and broken symmetry (BS), for two systems p-C₈H₈ and Cu₂Cl₆²⁻. The results are summarized in Table III.

The error in the energy difference between different spin states in both cases is much smaller than the error in total energy alone by $1 \sim 2$ orders of magnitude, with the error percentage only about 0.01%, as it is often easier to achieve higher accuracy in energy difference than in total energy alone. This makes the method particularly useful for studying properties involving energy difference such as exchange coupling or magnetic anisotropy energy (MAE). The similar pattern for the energy difference is also observed in Ref. [29].

An additional test for l -dependency is shown in Fig. 6 for (a) the total energy of Glycine and (b) the total energy

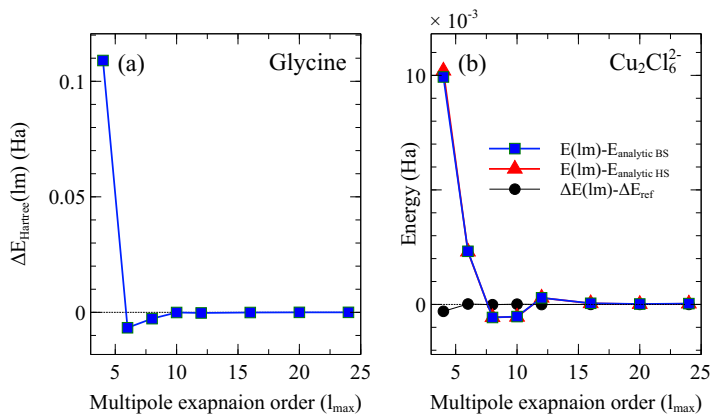


FIG. 6: Convergence versus multipolar expansion order l for (a). the total energy error of Glycine compared to the reference value and (b). the error of total energy of $\text{Cu}_2\text{Cl}_6^{2-}$ of both HS and BS spin states and of the energy difference between the two.

of $\text{Cu}_2\text{Cl}_6^{2-}$ of both HS and BS states and the energy difference between two states. While all total energies requires around $l = 16$ to reach convergence, it requires only up to $l = 6$ (see Fig. 6(b)) to converge the energy difference. Similar patterns can also be found in many different contexts such as Brillouin zone integration in MAE.

V. CONCLUSIONS

To summarize, we have reviewed two major numerical schemes (FDM and GF) for solving Poisson equation. Both methods were analyzed with common numerical tricks to improve the efficiency. We observed that, given the same set of radial parameters, FDM appears to be more accurate describing the monopole ($l = 0$) but it inherits a serious issue coming from the multipolar contribution of mainly $l = 1$ and sometimes $l = 2$. We propose a hybrid scheme by combining the two approaches, where the radial potential of monopole (i.e. U_{00}) in spherical harmonic expansion is calculated using FDM while the rest of the higher order terms are calculated using GF's function integration. We then performed a series of tests on different systems and the convergence with difference numerical parameters to demonstrate effect of the implementation. The overall results suggest that the accuracy is improved in all the cases. More importantly our analysis show that like GF method, the proposed hybrid approach is free from error accumulation with system size and is more accurate for the monopole than the GF method. This observation and its favorable scaling especially when large basis sets are employed makes it an attractive method for studies on large complexes.

ACKNOWLEDGMENTS

The authors thank Prof. Axel Becke for the comments on the manuscript that helped in improving its clarity. Authors gratefully acknowledge Dr. Carlos M. Diaz for discussions and assistance with parallelization of the implementation. The computational resources from the Texas Advanced Computing Center are gratefully acknowledged. This work was supported by the US Department of Energy, Office of Science, Office of Basic Energy Sciences, as part of the Computational Chemical Sciences Program under Award No. DE-SC0018331.

DATA AVAILABILITY

The data that support the findings of this study are available from the corresponding author upon reasonable request

* pchang2@utep.edu

† rzope@utep.edu

- [1] T. Helgaker, P. Jorgensen, and J. Olsen, *Molecular electronic-structure theory* (John Wiley & Sons, 2014).
- [2] L. E. McMurchie and E. R. Davidson, *Journal of Computational Physics* **26**, 218 (1978).
- [3] S. Obara and A. Saika, *The Journal of chemical physics* **84**, 3963 (1986).
- [4] R. A. Friesner, *Chemical physics letters* **116**, 39 (1985).
- [5] B. I. Dunlap, J. Connolly, and J. Sabin, *The Journal of Chemical Physics* **71**, 3396 (1979).
- [6] B. Dunlap, *The Journal of Chemical Physics* **78**, 3140 (1983).
- [7] J. Mintmire and B. Dunlap, *Physical Review A* **25**, 88 (1982).
- [8] B. Dunlap, *Journal of Molecular Structure: THEOCHEM* **529**, 37 (2000).
- [9] V. Termath and N. C. Handy, *Chemical Physics Letters* **230**, 17 (1994).
- [10] L. G. CP975667RF32 and V. Rokhlin, *J. Comput. Phys* **73**, 325 (1987).
- [11] L. Greengard, *The rapid evaluation of potential fields in particle systems* (MIT press, 1988).
- [12] A. W. Appel, *SIAM Journal on Scientific and Statistical Computing* **6**, 85 (1985).
- [13] J. Barnes and P. Hut, *nature* **324**, 446 (1986).
- [14] M. C. Strain, G. E. Scuseria, and M. J. Frisch, *Science* **271**, 51 (1996).
- [15] K. E. Schmidt and M. A. Lee, *Journal of Statistical Physics* **63**, 1223 (1991).
- [16] A. D. Becke, *The Journal of Chemical Physics* **88**, 2547 (1988).
- [17] B. Delley, *The Journal of Chemical Physics* **92**, 508 (1990).
- [18] E. F. Valeev, "Libint: A library for the evaluation of molecular integrals of many-body operators over gaussian functions," <http://libint.valeev.net/> (2021), version 2.7.1.

- [19] Q. Sun, *Journal of Computational Chemistry* **36**, 1664 (2015).
- [20] J. D. Jackson, *Classical electrodynamics; 2nd ed.* (Wiley, New York, NY, 1975).
- [21] A. D. Becke and R. M. Dickson, *The Journal of Chemical Physics* **89**, 2993 (1988).
- [22] E. Posada, F. Moncada, and A. Reyes, *Journal of Chemical Physics* **148** (2018), 10.1063/1.5012521.
- [23] T. Shiozaki and S. Hirata, *Physical Review A - Atomic, Molecular, and Optical Physics* **76**, 1 (2007).
- [24] A. D. Becke, *International Journal of Quantum Chemistry* **36**, 599 (1989).
- [25] A. D. Becke, *The Journal of Chemical Physics* **145**, 194107 (2016).
- [26] A. D. Becke, *The Journal of Chemical Physics* **149**, 081102 (2018).
- [27] A. D. Becke, *The Journal of Chemical Physics* **150**, 241101 (2019).
- [28] M. Franchini, P. H. T. Philipsen, E. Van Lenthe, and L. Visscher, *Journal of Chemical Theory and Computation* **10**, 1994 (2014).
- [29] V. Blum, R. Gehrke, F. Hanke, P. Havu, V. Havu, X. Ren, K. Reuter, and M. Scheffler, *Computer Physics Communications* **180**, 2175 (2009).
- [30] G. t. Te Velde, F. M. Bickelhaupt, E. J. Baerends, C. Fonseca Guerra, S. J. van Gisbergen, J. G. Snijders, and T. Ziegler, *Journal of Computational Chemistry* **22**, 931 (2001).
- [31] M. Franchini, P. H. T. Philipsen, and L. Visscher, *Journal of Computational Chemistry* **34**, 1819 (2013).
- [32] G. Te Velde and E. Baerends, *Physical Review B* **44**, 7888 (1991).
- [33] R. R. Zope, Y. Yamamoto, C. M. Diaz, T. Baruah, J. E. Peralta, K. A. Jackson, B. Santra, and J. P. Perdew, *The Journal of Chemical Physics* **151**, 214108 (2019).
- [34] V. I. Lebedev, *USSR Computational Mathematics and Mathematical Physics* **16**, 10 (1976).
- [35] A. El-Sherbiny and R. A. Poirier, *Journal of Computational Chemistry* **25**, 1378 (2004).
- [36] P. M. Gill, B. G. Johnson, and J. A. Pople, *Chemical Physics Letters* **209**, 506 (1993).
- [37] P. M. Gill and S. H. Chien, *Journal of Computational Chemistry* **24**, 732 (2003).
- [38] K. Kakhiani, K. Tsereteli, and P. Tsereteli, *Computer Physics Communications* **180**, 256 (2009).
- [39] M. Krack and A. M. Köster, *Journal of Chemical Physics* **108**, 3226 (1998).
- [40] R. Lindh, P. Å. Malmqvist, and L. Gagliardi, *Theoretical Chemistry Accounts* **106**, 178 (2001).
- [41] M. E. Mura and P. J. Knowles, *Journal of Chemical Physics* **104**, 9848 (1996).
- [42] C. W. Murray, N. C. Handy, and G. J. Laming, *Molecular Physics* **78**, 997 (1993).
- [43] O. Treutler and R. Ahlrichs, *The Journal of Chemical Physics* **102**, 346 (1995).
- [44] R. E. Stratmann, G. E. Scuseria, and M. J. Frisch, *Chemical Physics Letters* **257**, 213 (1996).
- [45] H. Gharibnejad, N. Douguet, B. I. Schneider, J. Olsen, and L. Argenti, *Computer Physics Communications* **263** (2021), 10.1016/j.cpc.2021.107889, arXiv:2101.08678.
- [46] H. Laqua, J. Kussmann, and C. Ochsenfeld, *Journal of Chemical Physics* **149** (2018), 10.1063/1.5049435.
- [47] G. Arfken, *Mathematical Methods for Physicists*, 3rd ed. (Academic Press, Inc., San Diego, 1985).
- [48] D. Porezag and M. R. Pederson, *Phys. Rev. A* **60**, 2840 (1999).
- [49] G. von Winckel, Greg von Winckel (2022). Finite Difference Weights (<https://www.mathworks.com/matlabcentral/fileexchange/5269-finite-difference-weights>), MATLAB Central File Exchange. Retrieved February 2, 2022. (2022).
- [50] W. H. Press, B. P. Flannery, S. A. Teukolsky, and W. T. Vetterling, *Numerical Recipes in FORTRAN 77: The Art of Scientific Computing*, 2nd ed. (Cambridge University Press, 1992).
- [51] J. P. Perdew and A. Zunger, *Physical Review B* **23**, 5048 (1981).
- [52] O. A. Vydrov, G. E. Scuseria, J. P. Perdew, A. Ruzsinszky, and G. I. Csonka, *The Journal of chemical physics* **124**, 094108 (2006).
- [53] Y. Yamamoto, S. Romero, T. Baruah, and R. R. Zope, *The Journal of Chemical Physics* **152**, 174112 (2020).